Rainfall erosivity mapping over mainland China based on high density hourly rainfall records

Tianyu Yue[1], Shuiqing Yin[1], Yun Xie[1], Bofu Yu[2], Baoyuan Liu[1]

[1]State Key Laboratory of Earth Surface Processes and Resource Ecology, Faculty of Geographical Science, Beijing Normal University, Beijing, 100875, China
[2]Australian Rivers Institute, School of Engineering and Built Environment, Griffith University, Nathan, Queensland, QLD 4111, Australia

Correspondence to: Shuiqing Yin (yinshuiqing@bnu.edu.cn)

Abstract. Rainfall erosivity quantifies the effect of rainfall and runoff on the rate of soil loss. Maps of rainfall erosivity are needed for erosion assessment using the Universal Soil Loss Equation (USLE) and its successors. To improve erosivity maps that are currently available, hourly and daily rainfall data from 2,381 stations for the period 1951-2018 were used to generate new R-factor and 1-in-10-year event EI_{30} maps for mainland China (available at https://dx.doi.org/10.12275/bnu.clicia.rainfallerosivity.CN.001; Yue et al., 2020). One-min rainfall data from 62 stations, of which 18 had a record length > 29 years, were used to compute the 'true' rainfall erosivity against which the new R-factor and 1-in-10-year EI_{30} maps were assessed to quantify the improvement over the existing maps through cross-validation. The results showed that (1) existing maps underestimated erosivity for most of the south-eastern part of China and overestimated for most of the western region; (2) the new R-factor map generated in this study had a median absolute relative error of 16% for the western region, compared to 162% for the existing map, and 18% for the rest of China. The new 1-in-10-year EI_{30} map had a median absolute relative error of 14% for the central and eastern regions of China, compared to 21% for the existing map (map accuracy was not evaluated for the western region where the 1-min data were limited); (3) the R-factor map was improved mainly for the western region, because of an increase in the number of stations from 87 to 150 and temporal resolution from daily to hourly; (4) the benefit of increased station density for erosivity mapping is limited once the station density reached about 1 station per 10,000 km^2.

1 Introduction

Soil erosion has been a major threat to soil health, soil and river ecosystem services in many regions of the world (FAO, 2019a). Soil erosion has on-site impacts, such as the reduction of soil and water, the loss of soil nutrients, the decrease of land quality and food production, as well as off-site impacts, such as excessive sedimentation and water pollution.

Soil erosion models are tools to evaluate the rate of soil loss and can provide policymakers useful information for taking measures in soil and water conservation. The Universal Soil Loss Equation (USLE; Wischmeier and Smith, 1965; 1978) and the Revised USLE (RUSLE; Renard et al., 1997; USDA-ARS, 2013) have been widely used to estimate soil erosion in at least

109 countries over the past 40 years (Alewell et al., 2019). Rainfall erosivity is one of the factors in the USLE and RUSLE to represent the potential ability of rainfall and runoff to affect soil erosion.

In the USLE, erosivity of a rainfall event is identified as the EI value, also denoted as EI_{30}, which is the product of the total storm energy (E) and the maximum 30-min intensity (I_{30}) (Wischmeier, 1959). The erosivity factor (R-factor) in the USLE is the mean annual total EI values of all erosive events. To recognize interannual rainfall variability, rainfall data of long periods are required (Wischmeier and Smith, 1978). In the original isoerodent maps generated by Wischmeier and Smith (1965), stations with rainfall data of at least 22 years were used.

To use the USLE, two additional input parameters are required. One is the seasonal distribution of the R-factor. To compute the soil erodibility factor (K-factor) and cover-management factor (C-factor), seasonal distribution of EI (monthly, Wischmeier and Smith, 1965; or half-month percentage of EI, Wischmeier and Smith, 1978; Renard et al., 1997) is needed. In addition, 1-in-10-year storm EI value (called "10-yr EI" in Renard et al. (1997)) is needed to compute the support practice factor (P-factor) for the contour farming (Renard et al., 1997).

Kinetic energy generated by raindrops can be calculated based on raindrop disdrometer data and estimated based on breakpoint or hyetograph data via KE-I equations, while I_{30} is expected to be prepared using breakpoint or hyetograph data with an observed interval $\leq$ 30 min. In the original study of event rainfall erosivity, the recording-rain-gauge chart was used (Wischmeier and Smith, 1958). However, these data were usually in shortage not only in the length but also in the spatial coverage.

Methods to estimate rainfall erosivity based on more readily available data have been developed widely, such as daily (Richardson et al., 1983; Haith and Merrill, 1987; Sheridan et al., 1989; Selker et al., 1990; Bagarello and D'asaro, 1994; Yu and Rosewell, 1996b, c; Zhang et al., 2002; Capolongo et al., 2008; Angulomartínez and Beguería, 2009; Xie et al., 2016), monthly (Arnoldus, 1977; Ferro et al., 1991; Renard and Freimund, 1994), and annual rainfall (Yu and Rosewell, 1996a; Ferrari et al., 2005; Bonilla and Vidal, 2011; Lee and Heo, 2011). Yin et al. (2015) evaluated a number of empirical models to estimate the R-factor using rainfall data of temporal resolutions from daily to average annual, and showed that the most accurate prediction was based on data at the highest temporal resolution.

Once values of the erosivity factor is obtained with site observations, spatial interpolation methods can be used to estimate rainfall erosivity for sites without rainfall data based on surrounding sites to produce the erosivity maps or isoerodent maps. Local values of erosivity can be taken from these maps (Wischmeier and Smith, 1978). Rainfall erosivity maps can also be meaningful in various fields such as soil erosion, sediment yield, environment and ecology. In the original version of the USLE, 181 stations with breakpoint data plus 1,700 stations with annul averaged precipitation, 1-in-2-year 1-h rainfall amount and 1-in-2-year 24-h amount were used to generate the erosivity map for the eastern part of the US (Wischmeier and Smith, 1965). In the successor of the USLE (Wischmeier and Smith, 1978), the erosivity map for the western part of the US were generated based on 1-in-2-year, 6-h rainfall amount data (P) using the equation of $R=27.38P^{2.17}$. In Revised USLE (RUSLE), Renard et al. (1997) released the erosivity map using the same data as Wischmeier and Smith (1965) for the eastern part, and 60-min rainfall data at 790 stations for the western part in the US. In RUSLE2, monthly erosivity maps based on 15-min data from

65   3,700 stations were generated (USDA-ARS, 2013). Erosvity maps based on spatial interpolation have been widely produced globally (Lu and Yu, 2002; Oliveira et al., 2012; Liu et al., 2013; Klik et al., 2015; Panagos et al., 2015a; Panagos et al., 2015b; Borrelli et al., 2016; Qin et al., 2016; Panagos et al., 2017; Sadeghi et al., 2017; Yin et al., 2019; Riquetti et al., 2020; Silva et al., 2020).

Recently, the Food and Agriculture Organization (FAO) proposed to produce a Global Soil Erosion Map (GSERmap) which

70   encouraged scientists around the world to generate their own national level maps making the most of the country knowledge, locally available methods and input data (FAO, 2019b). Rainfall erosivity maps for China were reviewed and relevant information on how they were generated are presented in Table 1, which shows that current R-factor maps for mainland China typically used readily-available daily rainfall data from about 500-800 stations (e.g. Zhang et al., 2003; Liu et al., 2013; Qin et al., 2016; Yin et al., 2019; Liu et al., 2020), which were recorded by simple rain gauges. However, daily rainfall data are

75   not enough to derive sub-daily intensities, which reduced the accuracy of estimated rainfall erosivity (Yin et al., 2015). One-minute data are the finest resolution data measured by automatic tipping bucket rain gauges we can obtain up to now, therefore they are one of the best datasets for deriving precipitation intensity and estimating rainfall erosivity. However, 62 stations with 1-min data collected were inadequate for the spatial interpolation of rainfall erosivity over mainland China. Hourly data was believed to reflect the temporal variation of precipitation intensity better than daily data, which can be used to improve the

80   estimation of at-site rainfall erosivity with precipitation observations. In addition, the increase of station density for the interpolation can better describe the spatial variation of rainfall erosivity and improve the estimation of rainfall erosivity for areas without observations together with the improvement of interpolation models and procedures.

Therefore hourly and daily data for more than 2,000 stations were collected, together with the 1-min data for 62 of them to: (a) develop high-quality maps of the R-factor and 1-in-10-year EI_{30} over the mainland China; (b) quantify the improvement of the

85   new erosivity maps using precipitation data in a higher temporal resolution and from more weather stations, and better interpolation techniques compared to those used to generate erosivity maps that are currently available (Yin et al., 2019). New R-factor and 1-in-10-year EI_{30} maps were produced in this study may improve the estimation of the soil loss in mainland China. The meaning and rationale of the study is to: (1) present and share high-precision maps of the R-factor and 1-in-10-year EI_{30} over the mainland China with related Earth system science communities; (2) provide some insights in the improvement of

90   rainfall erosivity maps for other regions.

Table 1: Studies on the mapping of R-factor for or involving China

Study Area	Period	Temporal resolution of precipitation data	No. of stations	Interpolation method	Reference
China	1956-1984	Multi-year average of annual, maximum daily and maximum hourly	125	Unknown	Wang et al., 1996
	1971-1998	Daily	564	Ordinary Kriging	Zhang et al., 2003
	1960-2009	Daily	590	Ordinary Kriging	Liu et al., 2013

Study Area	Period	Temporal resolution of precipitation data	No. of stations	Interpolation method	Reference
	1951-2010	Daily	756	Universal co-kriging with the aid of the elevation	Qin et al., 2016
	1961-2016	Daily	774	Ordinary Kriging	Yin et al., 2019 [*]
Global	1989-2010	Annual average	Gridded (0.5°×0.5°)	——	Naipal et al., 2015
	1998-2012 (in China)	Hourly and sub-hourly	3,625 (387 in China)	Gaussian Process Regression	Panagos et al., 2017
	1980-2017	Daily	30,000+ (~800 in China)	Thin-plate spline smoothing	Liu et al., 2020

*Map of 1-in-10-year EI_{30} in China was also generated.

2 Data and methods

95 ### 2.1 Data

2.1.1 Rainfall data

Rainfall data were obtained at the daily, hourly and 1-min intervals.

Daily rainfall data from 2,381 meteorological stations over mainland China (Fig.1) over the period of 1951-2014 was measured with simple rain gauges. The data were collected and quality controlled by the National Meteorological Information Center of

100 China Meteorological Administration. Daily data were collected all year around at these stations. An effective year of the daily data was defined as a year when there was no missing data for one or more months in the year, and a missing month was defined as a month when there were more than 6 missing days in the month. The missing records in the effective years were input as zero. Based on this definition, the number of effective years ranged from 18 to 54 years. Most of the stations (88%) have data of more than 50 years.

105 Hourly rainfall data from the same 2,381 stations with daily data (Fig. 1) were collected by siphon rain gauges or tipping bucket rain gauges and also quality controlled by the National Meteorological Information Center of China Meteorological Administration. The period of record for hourly data was from 1951 to 2018. The start year of the data varied because data collection commenced in different years. Observation was suspended in the snowy season, which resulted in some missing months in winter for station in the northern part of China. There were 932 (39%) stations with data for the whole year, 550 (23%) stations

110 from April to October and 421 (18%) stations from May to September.
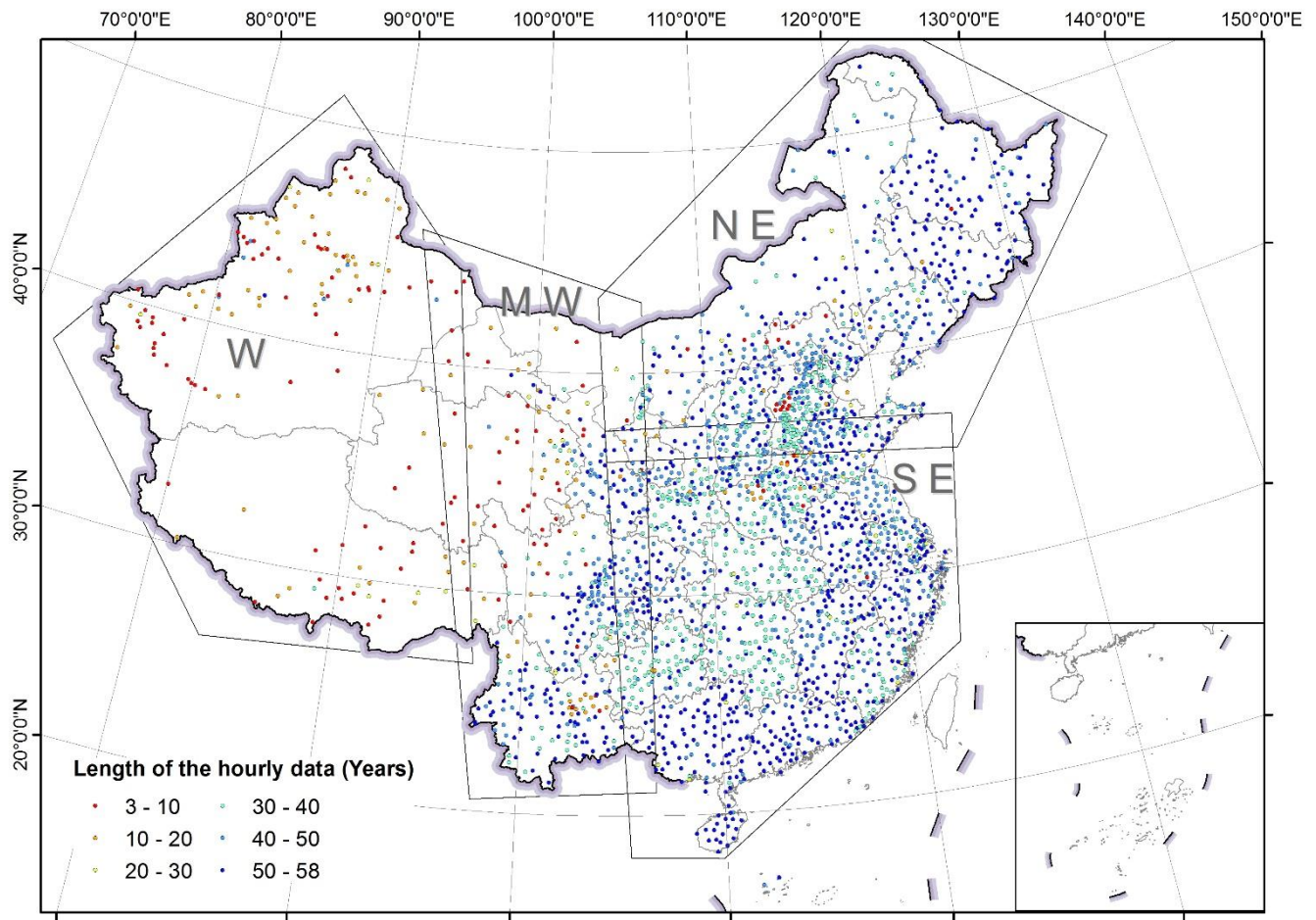
Figure 1: Spatial distribution of stations with daily and hourly rainfall data and the length of the hourly data. Western, Mid-western, North-eastern and South-eastern regions were abbreviated as W, MW, NE and SE, respectively.

The missing data were handled according to the following criteria: (a) a day with more than 4 missing hours was defined as a

115   missing day; (b) a month with more than 6 missing days was defined as a missing month; (c) a year with any missing month in its wet-season was defined as a missing year. The wet-season for stations north of 32 °N was from May to September, and for those south of 32 °N was from April to October. Missing years were removed and missing hours in the remaining effective years were input in two categories: (a) the missing period is followed by a non-zero record, which recorded the accumulated rainfall amount in the missing period based on data notes; (b) the missing period is followed by zero. In the first case, each

120   missing hour and the following non-zero hour were assigned the mean value of the non-zero record in these hours. For the second case, the missing hours were input as zero value.

Data at 1-min intervals were collected from 62 stations in mainland China (Fig. 2; and were used in Yue et al., 2020). Data from station No. 1-18 have effective years of 29-40 and cover the period of 1961(1971)-2000. Data from stations No. 19-62 have effective years of 2-12 and cover the period of 2005-2016. The missing data in the effective years were assumed to be zero.
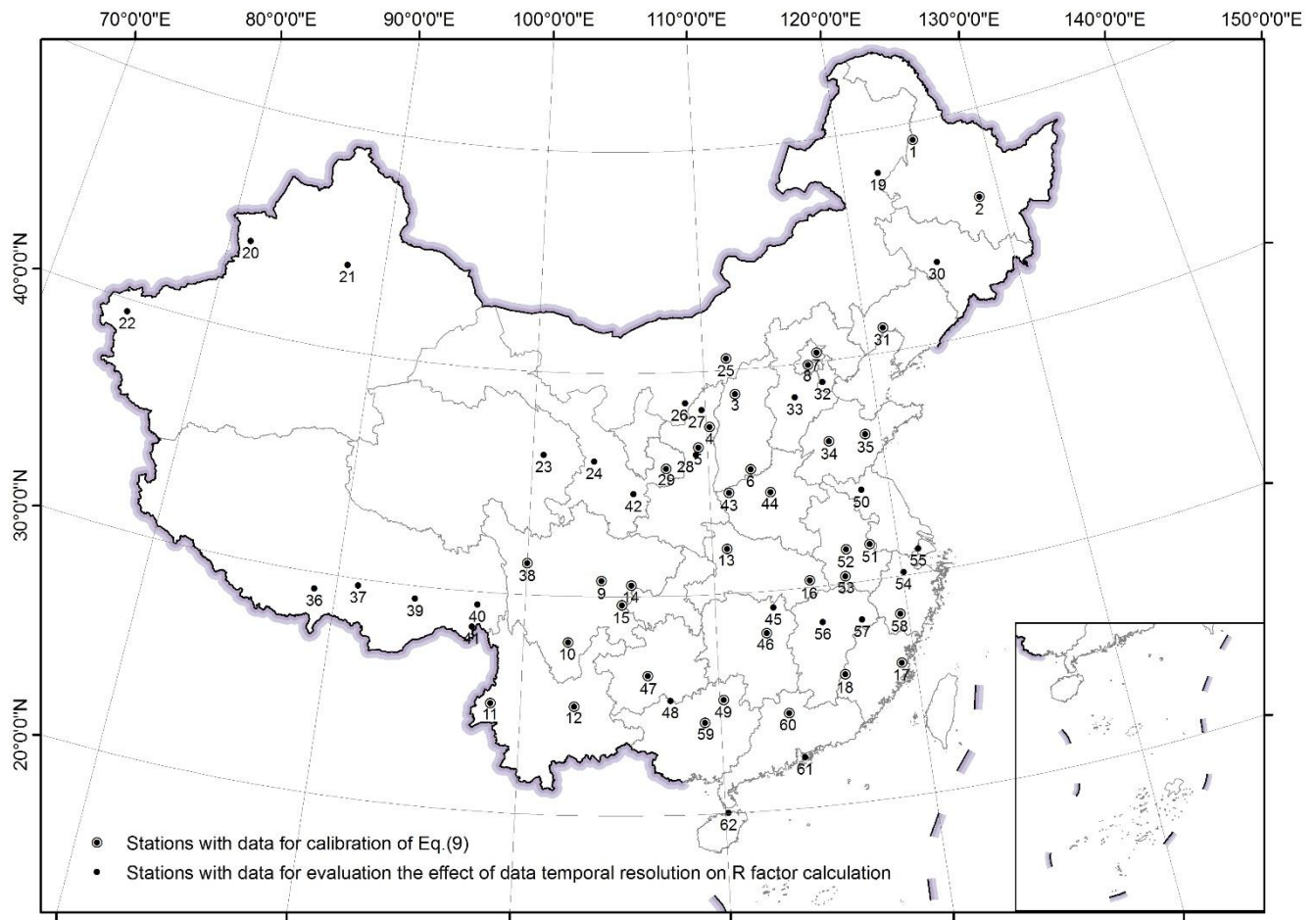
5

125

Figure 2: Spatial distribution of the stations with 1-min rainfall data

2.1.2 Published rainfall erosivity maps for China

The existing rainfall erosivity maps were collected and compared with the maps generated in this study. The current national R-factor map and 1-in-10-year EI_{30} map are based on daily rainfall data only over the period from 1961 to 2016 from 774

130 stations in China (Yin et al., 2019). Another R-factor map shown in the discussion section of this study (Fig. 12) was based on the global rainfall erosivity dataset published by Joint Research Centre - European Soil Data Centre (ESDAC; Panagos et al., 2017).

2.2 Calculation of rainfall erosivity using 1-min, hourly and daily data

One-minute and hourly data were first separated into storm events. A continuous period of >= 6 hours of no-precipitation was

135 used to separate storms (Wischmeier and Smith, 1978). Storms with the amount of >= 12 mm were defined as erosive events (Xie et al., 2000), and were used to calculate the rainfall erosivity factors.

6

The R-factor was calculated using Eqs. (1-3; USDA-ARS, 2013):

$$R = \frac{1}{N}\sum_{i=1}^{N}\sum_{j=1}^{m}(EI_{30})_{ij},\tag{1}$$

$$E = \sum_{r=1}^{l}(e_r \cdot P_r),\tag{2}$$

$$e_r = 0.29[1 - 0.72exp(-0.082i_r)],\tag{3}$$

where EI_{30} (event rainfall erosivity, MJ mm ha^{-1} h^{-1}) was the product of the total storm energy E (MJ ha^{-1}) and the maximum 30-min intensity I_{30} (mm h^{-1}); i=1, 2, …, N, where N is the number of effective years, and j = 1, 2, …, m means there are m erosive storm events in the ith year. For each storm event, rainfall was divided into l time intervals depending on the temporal resolution of rainfall data. The total storm energy E was the sum of the energy for each time interval r, which was the unit energy e_r (energy per mm of rainfall, MJ ha^{-1} mm^{-1}) multiplied by the rainfall amount P_r (mm) for each time interval. And i_r was the intensity (mm h^{-1}) of the rth interval. I_{30} (mm h^{-1}) was the maximum intensity over 30 consecutive minutes for each storm event. For hourly data, the I_{30} was assumed to be the same as the maximum 1-hour intensity.

The 1-in-10-year EI_{30} with 1-min or hourly data was obtained by fitting the generalized extreme value distribution (GEV). The GEV distribution is a family of probability distributions of Gumbel, Fréchet and Weibull, and can be denoted as G (μ, σ, ξ) with parameters μ (location), σ (scale), and ξ (shape) (Coles, 2001):

$$G(z) = exp\left\{-\left[1 + \xi\left(\frac{x-\mu}{\sigma}\right)\right]^{-1/\xi}\right\}\{x: 1 + \xi(x - \mu)/\sigma > 0\},\tag{4}$$

where x was the annual maximum storm EI_{30} (MJ mm ha^{-1} h^{-1}), $-\infty < \mu < \infty$, $\sigma > 0$ and $-\infty < \xi < \infty$. The extreme quantiles of the annual maximum EI_{30} (X_p) can be obtained by inverting Eq. (4):

$$X_p = \begin{cases} \mu - \frac{\sigma}{\xi}\left[1 - \{-\log(1 - p)\}^{-\xi}\right], for\ \xi \neq 0 \\ \mu - \sigma\log\{-\log(1 - p)\}, \ for\ \xi = 0 \end{cases},\tag{5}$$

where $G(X_p) = 1 - p$. The 1-in-10-year EI_{30}, was the value of X_p when p was 1/10.

Parameter values for the GEV distribution were estimated using the L-moments method (Hosking, 1990).

Since hourly data aggregation of 1-min data and temporal variation in rainfall intensity is reduced, erosivity factor values computed with hourly data would be underestimated. Therefore, the R-factor and 1-in-10-year EI_{30} values computed with hourly data need to be adjusted by multiplying conversion factors of 1.871 and 1.489 (SI units), which were fitted by 1-min rainfall data from 62 stations over mainland China (Yue et al., 2020). Erosivity factors from daily data were also obtained as described in Section 2.3. The R-factor using daily data was the mean annual daily erosivity. Daily rainfall erosivity was obtained by the following equation developed by Xie et al. (2016):

$$R_{daily} = \alpha P_{daily}^{1.7265},\tag{6}$$

where P_{daily} was the daily precipitation ($\geq$ 10 mm), parameter α was 0.3937 in the warm season (May to September), and 0.3101 in the cold season (October to April).

The 1-in-10-year EI_{30} using daily data was the 1-in-10-year daily erosivity adjusted with a conversion factor of 1.17 based on 1-min data from 18 stations in China (Yin et al., 2019). And the 1-in-10-year daily erosivity was obtained by calibrating the GEV distribution parameters as Eqs. (4-5) and the x in the functions was replaced by the annual maximum daily erosivity.

2.3 Rainfall erosivity for individual stations

170   Hourly data from 2,381 stations were used to produce the R-factor and the 1-in-10-year EI_{30} maps. Due to the annual variability of rainfall erosivity, stations with less than 22 effective years should be excluded (Wischmeier and Smith, 1978). However, 133 out of 150 stations in western China have less than 22 effective years (Fig. 1). Once these stations are removed, the western stations would be too sparse, which would reduce the interpolation accuracy of the rainfall erosivity map. To fill the gap due to the insufficient number of years, daily rainfall data with longer periods of record were used to adjust erosivity values based

175   on hourly data at the same station.

When the effective years of hourly data were not less than those of daily data for 871 out of 2,381 station, no adjustment of the R-factor was made. For the remaining 1,510 stations, the R-factor from hourly data was then adjusted by a relationship between the mean annual rainfall and the R-factor computed with hourly data as follows (Zhu and Yu, 2015):

$$R_{\text{h\_adj}} = R_{hour} \left(\frac{P_d}{P_h}\right)^{1.481},$$ (7)

180   where $R_{\text{h\_adj}}$ was the adjusted R-factor, R_{hour} was the estimated R-factor using hourly rainfall data, P_d was the mean annual precipitation of longer period (period of the daily data), and P_h was the mean annual precipitation of shorter period (period of the hourly data).

The exponent value of 1.481 was estimated based on a power relationship between the mean annual precipitation and the R-factor, and the latter was determined using 1-min and daily rainfall data of 35 stations in China (Fig. 2). All the daily and 1-

185   min data shared common periods of record of more than 10 years.

$$R_{min} = 0.156 \cdot P_m^{1.481},$$ (8)

where R_{min} was the R-factor (MJ mm ha^{-1} h^{-1} a^{-1}), and P_m was the mean annual precipitation (mm) using 1-min data. The coefficient of determination (R^2) was 0.776 for Eq. (8).

The 1-in-10-year EI_{30} for the stations was adjusted in a similar fashion. No adjustment is needed for 89% of the stations where

190   the effective years of the hourly data were not less than 22 years. For the remaining 11% of the station, the 1-in-10-year EI_{30} was estimated with daily data.

The record length was 22 to 29 years for 16 (0.7%) stations, 30 to 39 years for 44 (1.8%) stations, 40 to 49 years for 216 (9.1%) stations, more than 50 years for 2,105 (88.4%) stations when these adjustments were made.

2.4 Spatial interpolation and cross validation

195   The erosivity maps were obtained using the method of Universal Kriging with the annual rainfall as a co-variable. The mean annual rainfall was computed using daily rainfall data and was interpolated using Ordinary Kriging, and interpolated mean

annual rainfall was then used to interpolate the R-factor value using Universal Kriging. Both the mean annual precipitation and the erosivity factor were interpolated first for each of the four regions separately (Fig. 1; Li et al., 2014), and then combined to obtain annual precipitation and erosivity maps over China. Buffer areas were used to avoid discontinuity along region boundaries (Li et al., 2014).

To evaluate the efficiency of interpolation models, a leave-one-out cross-validation method was applied to each region. Symmetric mean absolute percentage error (sMAPE) and Nash-Sutcliffe coefficient of efficiency (NSE) were used for the assessment:

$$\text{sMAPE} = \frac{1}{n}\sum_{i=1}^{n}\left|\frac{F_i - A_i}{(F_i + A_i)/2}\right| \times 100\%, \tag{9}$$

$$\text{NSE} = 1 - \frac{\sum_{i=1}^{n}(F_i - A_i)^2}{\sum_{i=1}^{n}(A_i - \bar{A_i})^2}, \tag{10}$$

where n was the number of stations, F_i was the estimated value through Universal Kriging for the ith station using data from surrounding stations, A_i was the observed value at the ith station.

2.5 Accuracy assessment of erosivity maps

To evaluate the accuracy of the new erosivity maps, erosivity factors using 1-min data were assumed as the "true" values to calculate relative errors since they are most accurate. For the R-factor, 1-min data for 62 stations were used. For 1-in-10-year EI_{30}, 1-min data for 18 stations (No. 1-18; Fig. 2) of the 62 stations with more than 22 years were used. The cross-validation results for these stations from the interpolation of the two erosivity maps were compared to the values from 1-min data to calculate relative errors. Since the relative error tends to be high for stations with small R-factor values, the overall relative error for erosivity maps was represented with the median of the absolute value of the relative error for all the stations.

2.6 Comparative evaluation of the existing and new erosivity maps

Existing erosivity mapping at the national scale in mainland China usually uses daily rainfall data from about 500-800 stations. The R-factor and 1-in-10-year EI_{30} maps of Yin et al. (2019) were taken as references to evaluate the improvement in the accuracy of the erosivity maps generated in this study. Their relative errors were also obtained with 1-min data as described above.

New erosivity maps in this study followed a procedure that is different from Yin et al. (2019) mainly in three aspects: (1) temporal resolution (hourly vs. daily); (2) number of stations (2,381 stations vs. 744 stations); (3) interpolation method (Universal Kriging vs. Ordinary Kriging).

To evaluate the effect of the temporal resolution on R-factor and 1-in-10-year EI_{30}, data from the same set of stations were used, and the only difference was that in temporal resolution. Hourly and daily rainfall data with the same period as the 1-min data at the 62 stations were used to calculate R-factors and 1-in-10-year EI_{30} respectively. Erosivity factors from 1-min data are regarded as the most accurate values. The relative errors of erosivity factors from daily and hourly data were computed for evaluating accuracy.

9

To evaluate the effect of station density, maps were compared with the only difference in the number of stations. Hourly data from 774 stations (the same set of stations in Yin et al., 2019) and from 2,381 stations (used in this study) were used to generate two separate erosivity maps. R-factor and 1-in-10-year EI_{30} values were compared using a leave-one-out cross validation method region by region. The sMAPE was calculated for accuracy assessment.

To evaluate the effect of interpolation methods, maps were compared with the only difference in interpolation methods. Ordinary Kriging and Universal Kriging with the mean annual rainfall as the co-variable were applied for the R-factor and 1-in-10-year EI_{30} computed using hourly data from 2,381 stations. Both interpolation methods were applied to each of four different regions as shown in Fig. 1 and leave-one-out cross validation results were compared. The sMAPE was calculated to evaluate the accuracy of interpolated values.

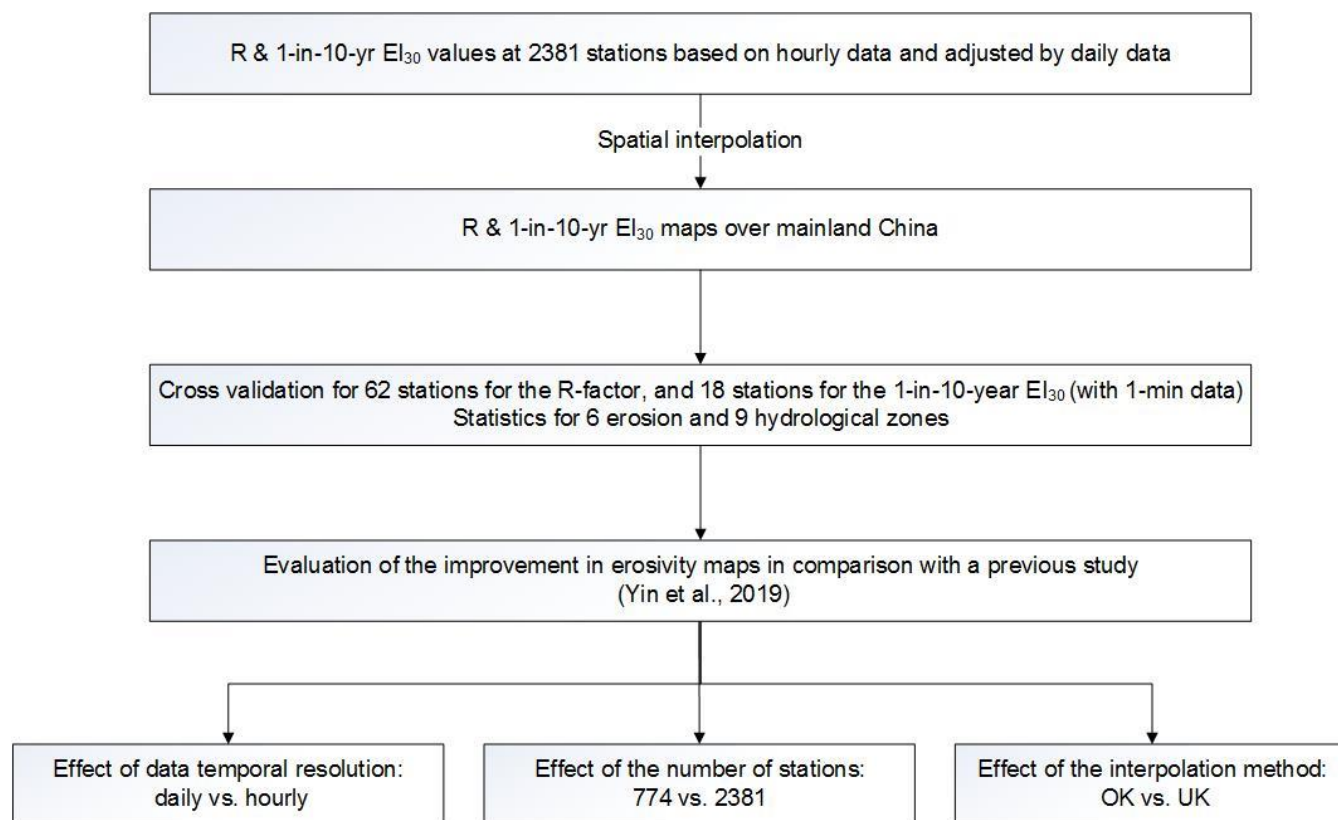The framework of this study is shown in Fig. 3.

Figure 3: Framework of this study

3 Results

### 3.1 Accuracy evaluation on erosivity maps

With erosivity maps from Yin et al. (2019) as references, this study shows improvement in the accuracy of estimated R-factor and 1-in-10-year EI_{30} (Fig. 4 and Fig.5; Table 2). The spatial distribution of the absolute relative errors of the maps from this study is shown in Fig. 6.

The R-factor values in the map of Yin et al. (2019) were underestimated where the R-factor was relatively high, and overestimated where the R-factor was relatively low. The improvement was particularly noticeable for western China (R < 1,000 MJ mm ha^{-1} h^{-1} a^{-1}) and the south-eastern coastal region (R > 10,000 MJ mm ha^{-1} h^{-1} a^{-1}).

Relative errors of erosivity factors at the stations from the two maps are shown in Fig. 5 (a) and (b). Those with the relative error of more than 100% were all in the Western (W) or Mid-western (MW) region. The absolute relative error for the R-factor in this study and Yin et al. (2019) was no more than 19% for Mid-western (MW), North-eastern (NE) and South-eastern (SE) regions (Table 2). However, there are some extremely high relative error values in Yin's map which were found to be located in the MW region (Fig. 5a). The median values of the absolute relative error in the R-factor in Western (W) region were 16.2% and 161.6%, respectively for this study and Yin et al. (2019). For 1-in-10-year EI_{30}, the median values of the absolute relative error were 13.5% for this study and 20.6% for Yin et al. (2019), indicating a smaller improvement in the mid-western and eastern regions compared to the improvement for the R-factor map (Table 2, (Fig. 5b). The relative errors of the 1-in-10-year EI_{30} in this study concentrated in the range of -10% ~ +10%, whereas those in Yin et al. (2019) concentrated in the range of -25% ~ -15% and +15% ~ +25% (Fig. 5c). The western region was excluded in the evaluation of the 1-in-10-year EI_{30} map because the record length of the 1-min data was too short to estimate 1-in-10-year event erosivity.
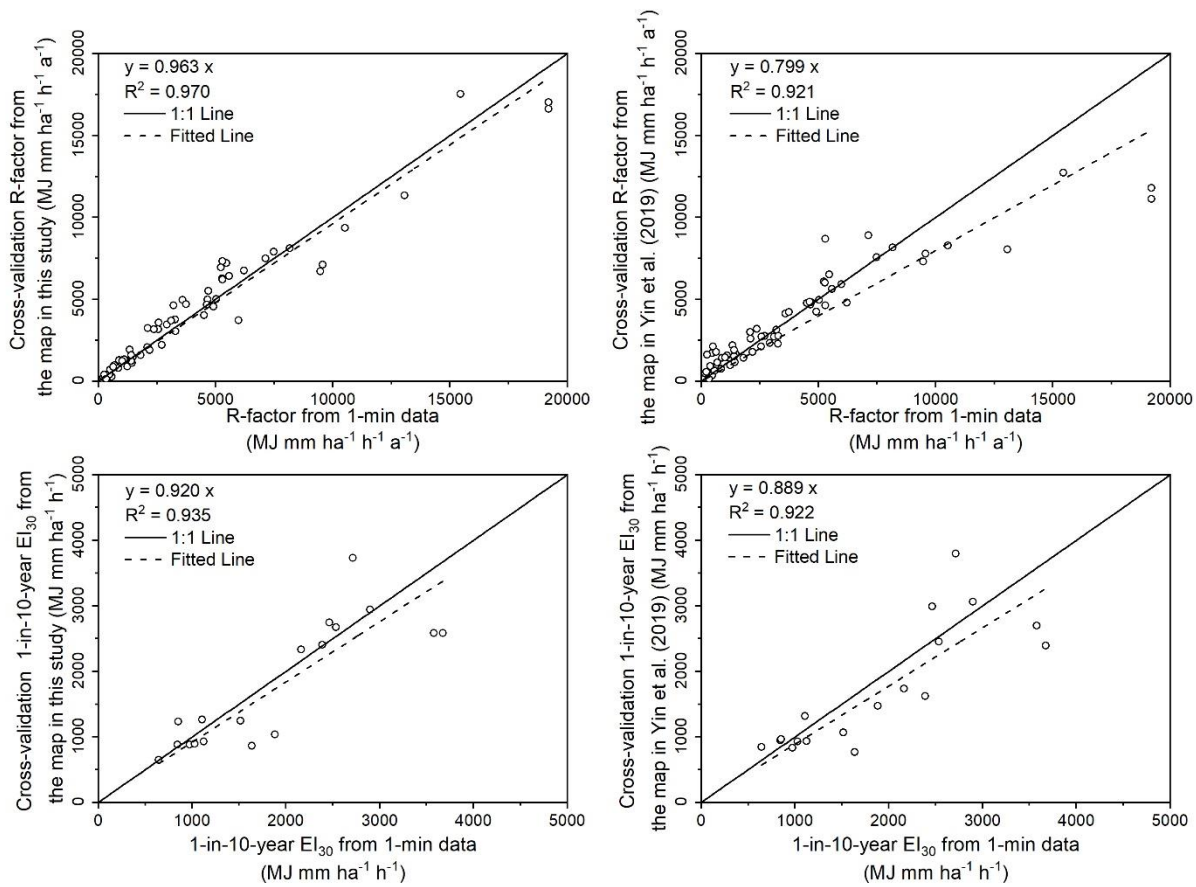
260　**Figure 4: Comparison of the R-factors and 1-in-10-year EI_{30} of the cross-validation values at the station of the maps and the values from 1-min data. The graphs on the left were the evaluation of the maps generated in this study, and those on the right were the evaluation of the maps generated by Yin et al. (2019)**
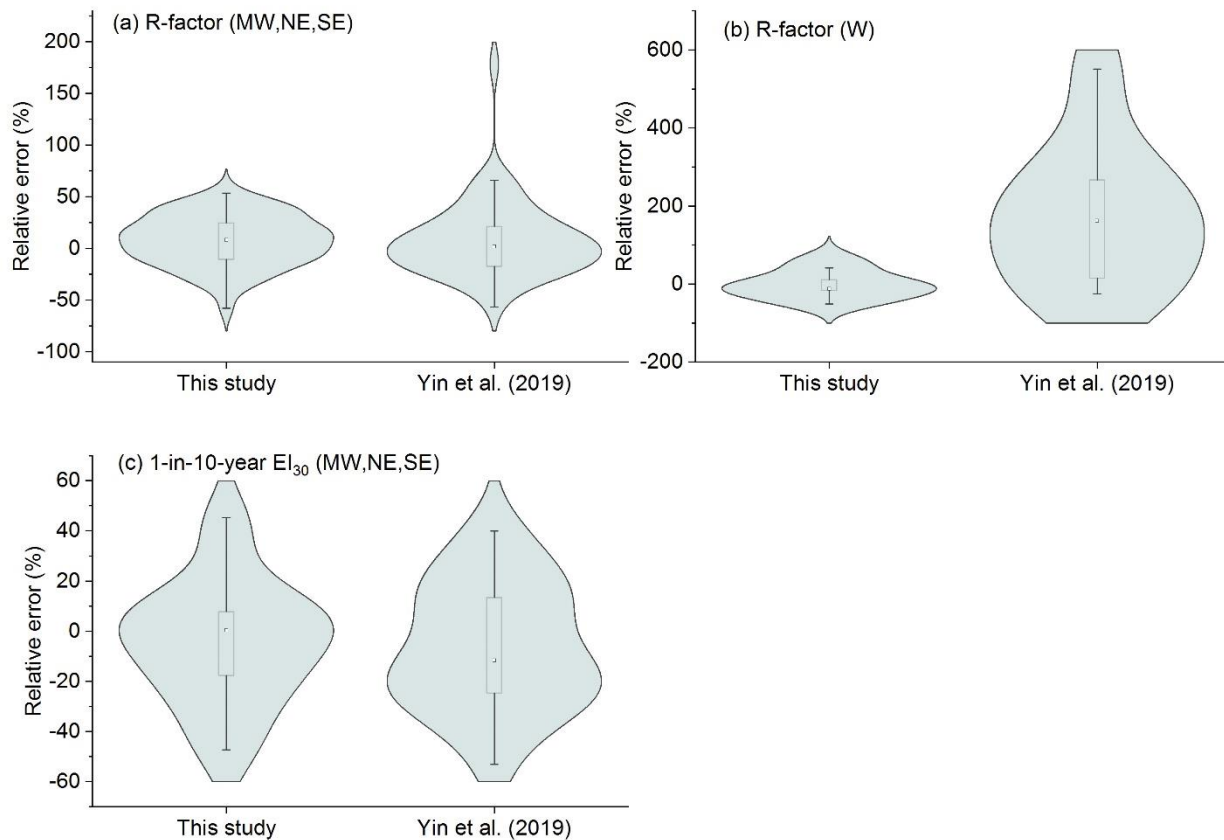
Figure 5: The relative errors of the R-factor (a for region MW, NE, SE; b for region W) and 1-in-10-year EI$_{30}$ (c for region ME, NE, SE) maps

Table 2: The statistical characteristics of the absolute relative errors of the erosivity factors from the maps

	R-factor				1-in-10-year EI$_{30}$	
	MW, NE, SE		W		MW, NE, SE	
	This study	Yin et al. (2019)	This study	Yin et al. (2019)	This study	Yin et al. (2019)
25th percentile	9.3%	8.8%	11.4%	23.1%	5.1%	13.0%
Median	17.8%	18.1%	16.2%	161.6%	13.5%	20.6%
75th percentile	32.8%	34.4%	45.9%	292.3%	31.6%	31.3%
Mean	21.0%	24.7%	28.7%	184.8%	18.6%	22.3%

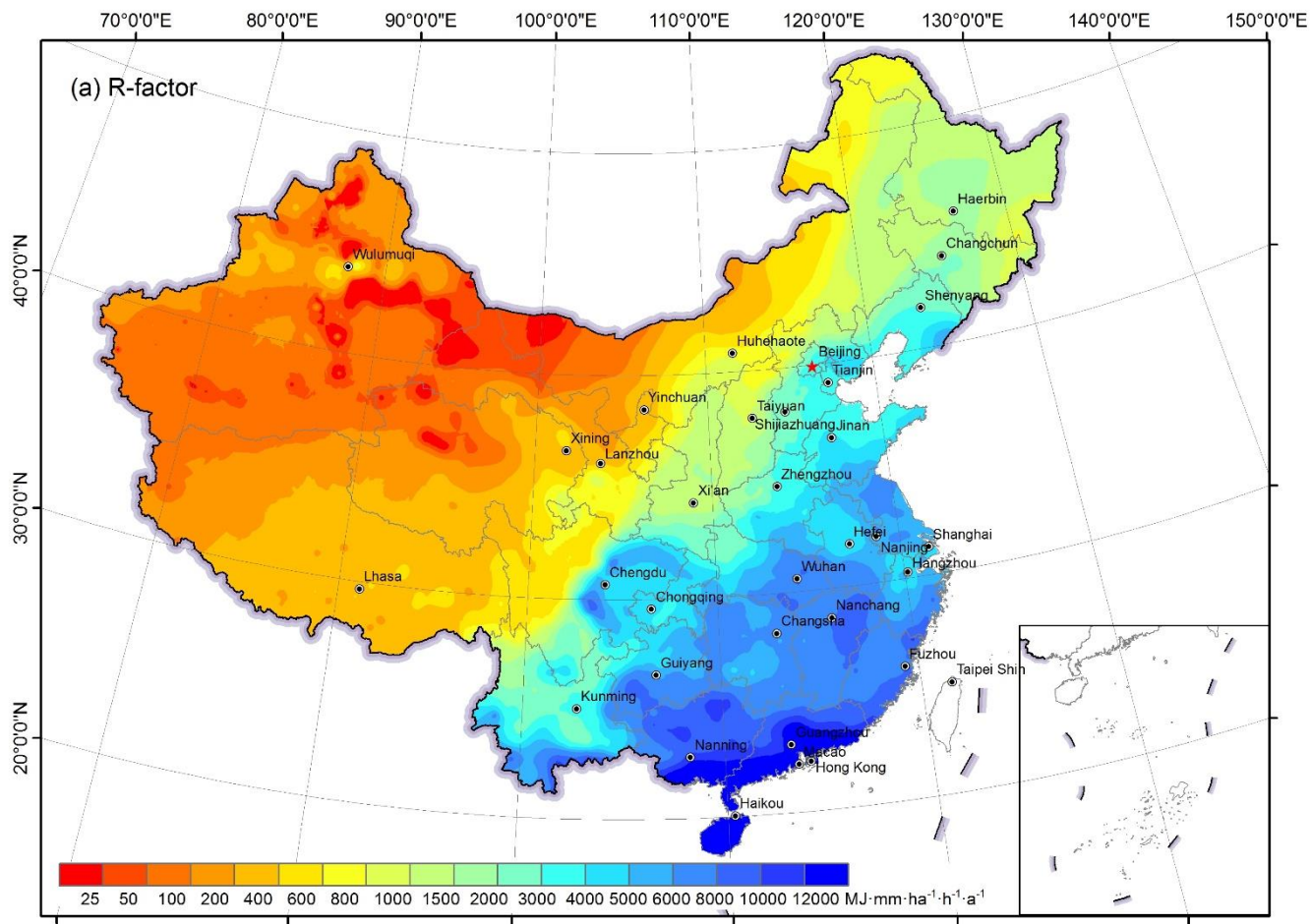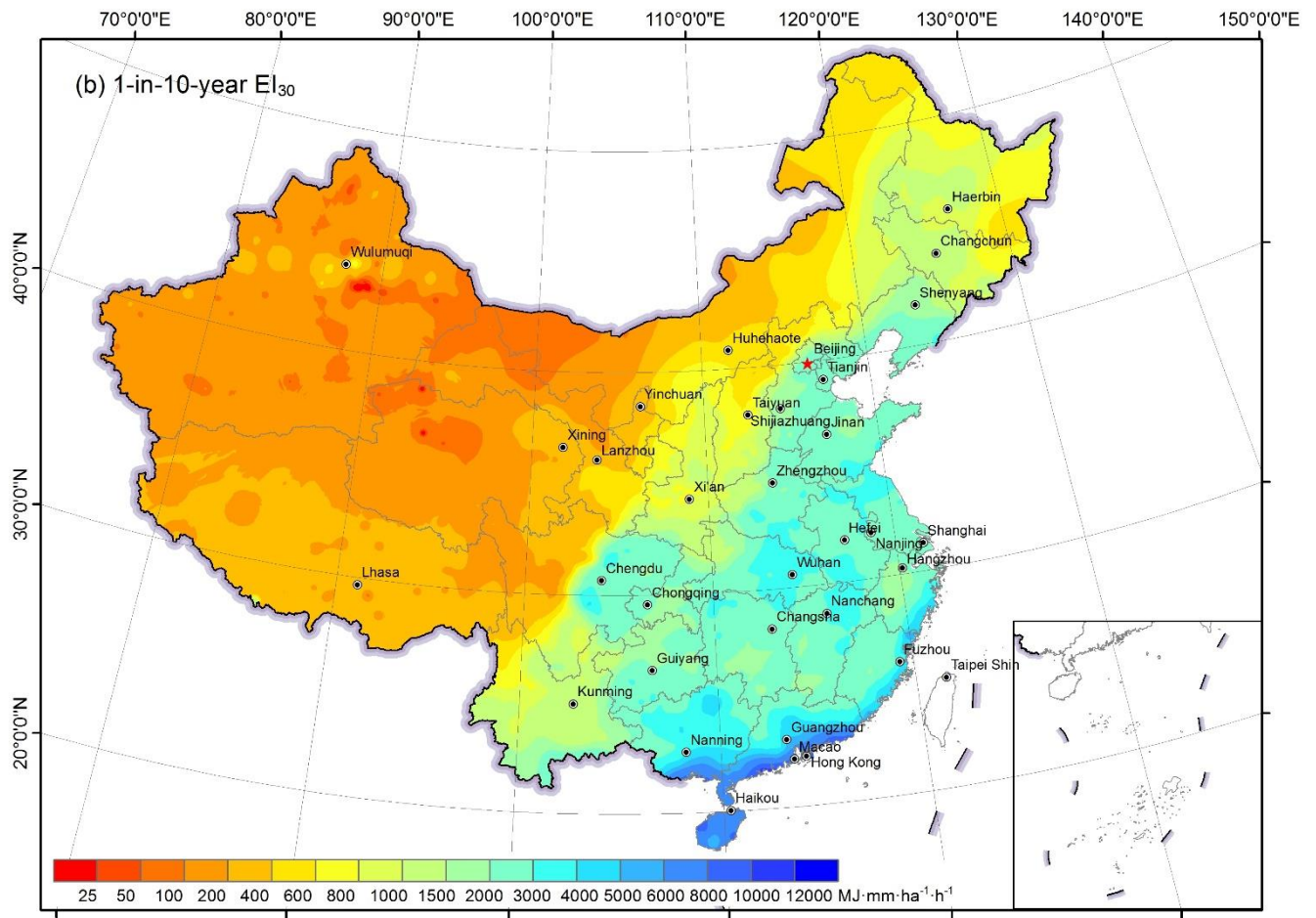270 **(a) R-factor**   **(b) 1-in-10-year EI$_{30}$**
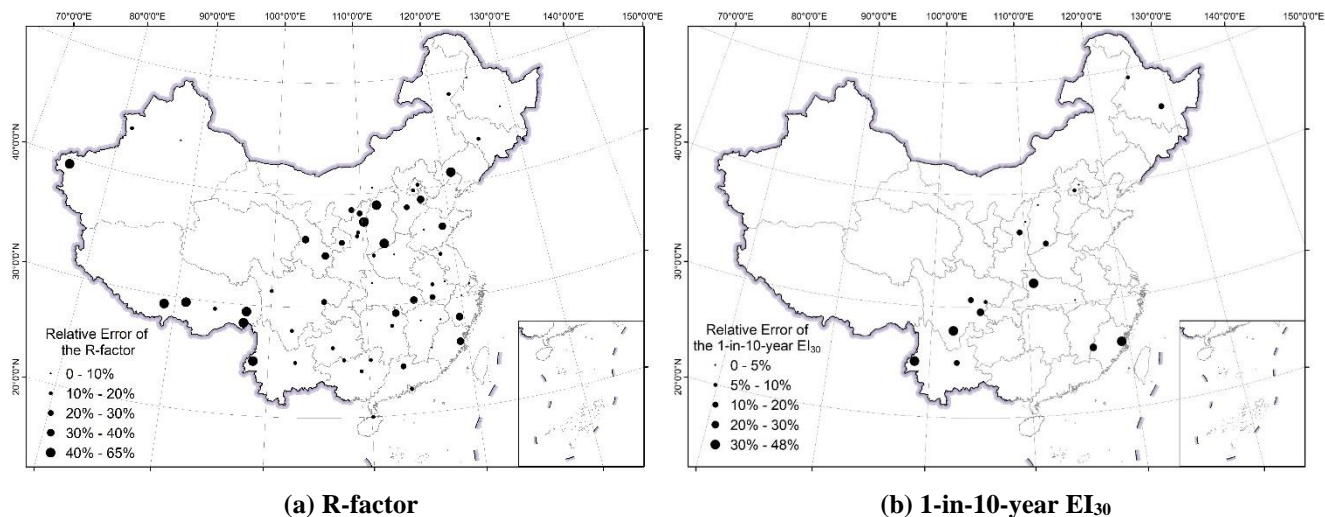
Figure 6: Spatial distribution of the absolute relative errors in the map of R-factor for 62 stations (a) and in the map of 1-in-10-year EI$_{30}$ for 18 stations (b) with 1-min observation data.

3.2 Erosivity maps and improvements over previous studies

The R-factor in China generally decreased from the south-eastern to the north-western (Fig. 7a), ranging from 0 to 25,300 MJ

275   mm ha^{-1} h^{-1} a^{-1}. The map of 1-in-10-year EI$_{30}$ shows a similar spatial pattern as that of the R-factor (Fig. 7b), ranging from 0 to 11,246 MJ mm ha^{-1} h^{-1}. Zero R-factor value is found at Turpan, Xinjiang Uygur Autonomous Region, where the mean annual rainfall is only 7.8 mm. The maximum of the R-factor (more than 20,000 MJ mm ha^{-1} h^{-1} a^{-1}) is found in the southern part of the Guangxi and Guangdong provinces, along the South China Sea, where the mean annual rainfall is more than 2,500 mm.

280   In addition to the overall trend, some local scale characteristics could be identified. For the R-factor map, in the western region, the wetter region in north-western China was located in the west of Dzungaria Basin and along the Tianshan Mountain, which has been captured on the map. Some statistical characteristics of the new maps of the erosivity factors are shown in Table 3 based for soil erosion and hydrological zones in China (Fig. 8).

14

(a) R-factor

(b) 1-in-10-year EI₃₀

25 50 100 200 400 600 800 1000 1500 2000 3000 4000 5000 6000 8000 10000 12000 MJ·mm·ha⁻¹·h⁻¹

Figure 7: R-factor(a) and 1-in-10-year EI₃₀(b) over mainland China based on hourly data from 2381 stations

(a) Soil erosion zoning

Non-water Erosion Region (NWE)
Northeastern Black Soil Region (NEB)
Northern Rock Soil Region (NR)
Northwestern Loess Plateau Region (NWL)
Southern Red Soil Region (SR)
Southwestern Rock Mountain Region (SWR)

(b) Hydrological zoning

Continental Basin
Haihe River Basin
Huaihe River Basin
Pearl River Basin
Songhua and Liaohe River Basin
Southeast Basin
Southwest Basin
Yangtze River Basin
Yellow River Basin
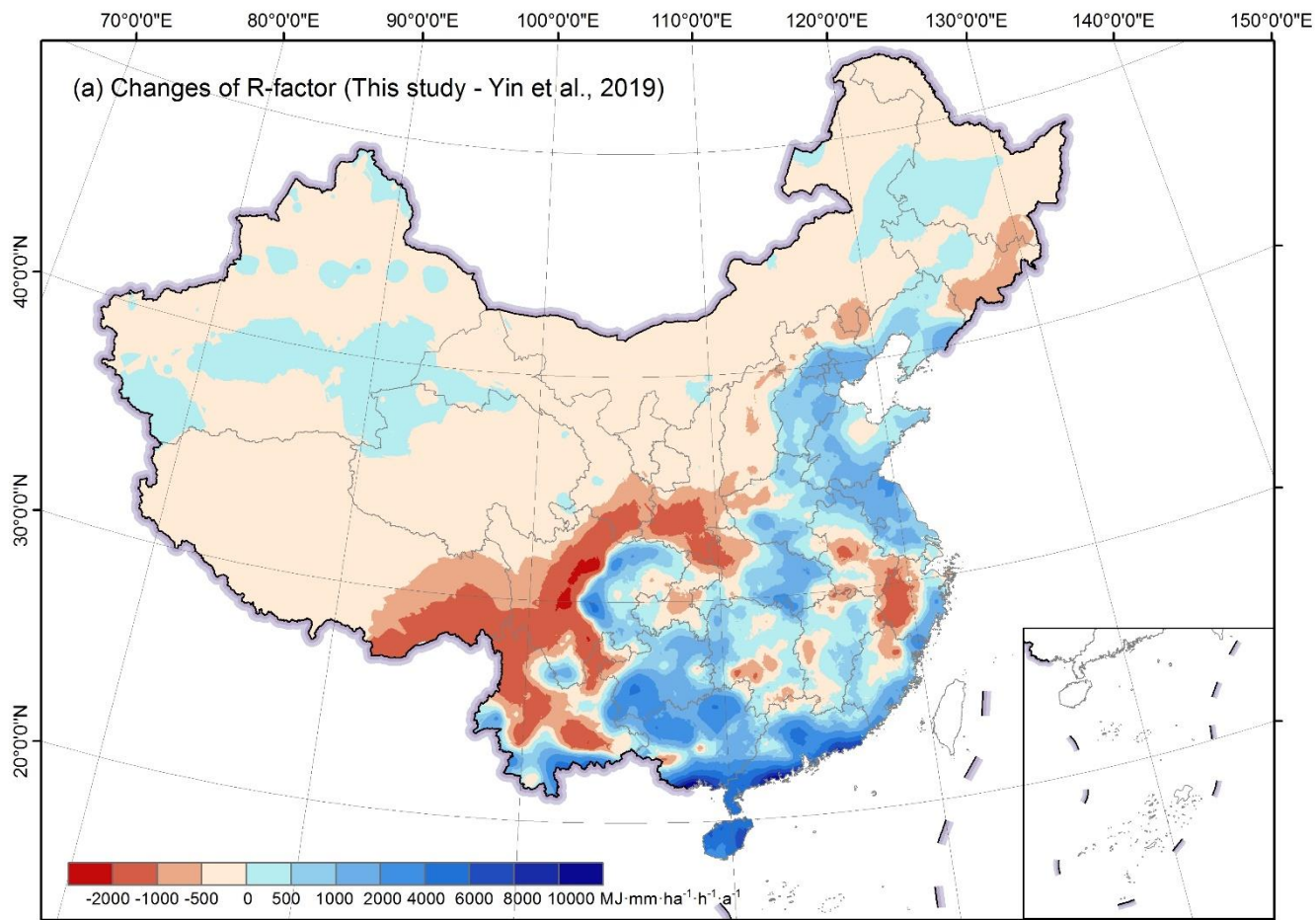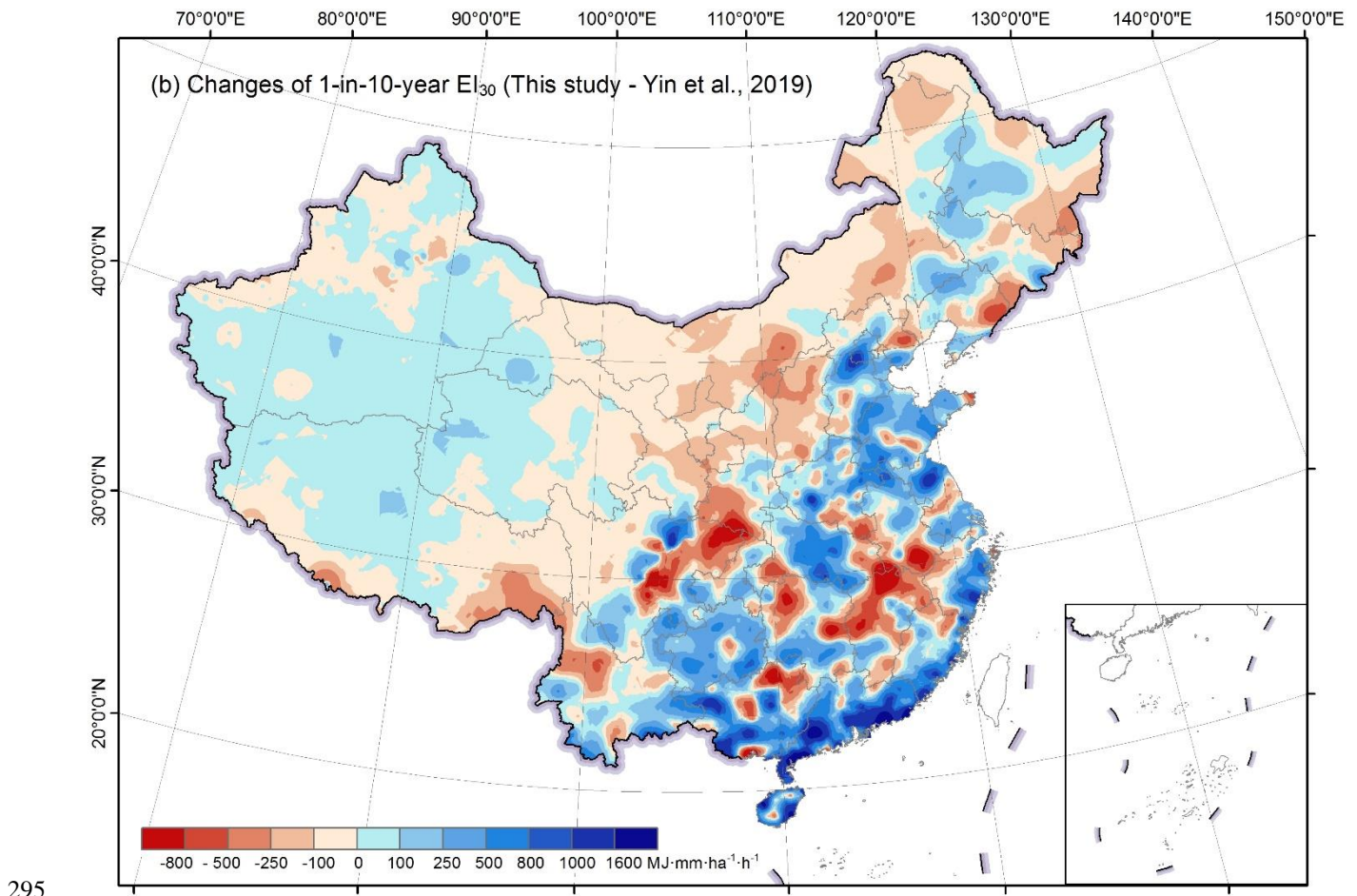
290   **Table 3: Statistical characteristics of R-factor and 1-in-10-year EI$_{30}$ in soil erosion and hydrological zonings**

Parameters	Zones	Mean	Std.	5th-percentile	25th-percentile	50th-percentile	75th-percentile	95th-percentile
R-factor (MJ mm ha^{-1} h^{-1} a^{-1})	Mainland China	2200	3147	47	147	645	3503	8208
	NWE	208	192	30	70	144	276	614
	NWL	896	431	263	549	875	1239	1562
	NR	3637	1443	935	2780	3747	4577	5946
	NEB	1483	766	671	1041	1311	1611	3284
	SWR	4226	2079	841	2610	4324	5503	8060
	SR	8294	3370	4918	6140	7311	9141	16544
	Continental	138	130	25	62	92	174	424
	Haihe	2437	1169	719	1218	2717	3489	4042
	Huaihe	4744	948	3197	4062	4653	5466	6310
	SongLiao	1405	765	623	952	1235	1553	3220
	Yellow	920	754	214	402	749	1205	2199
	Yangtze	3933	2535	215	1355	4508	6052	7666
	Southwest	1318	2043	132	265	316	940	5998
	Southeast	7069	1292	4964	6014	7192	7916	9110
	Pearl	10280	3967	4450	7697	9354	12731	
1-in-10-year EI$_{30}$ (MJ mm ha^{-1} h^{-1})	Mainland China	1040	1259	99	166	435	1766	3206
	NWE	189	101	84	125	165	220	415
	NWL	635	254	226	438	635	825	1031
	NR	2199	770	556	1860	2422	2717	3123
	NEB	948	449	444	669	867	1044	2055
	SWR	1706	766	439	1098	1689	2308	2952
	SR	3273	1418	1953	2375	2846	3512	6814
	Continental	164	84	80	114	140	193	363
	Haihe	1595	794	459	718	1773	2350	2626
	Huaihe	2706	394	1999	2465	2723	2957	3337
	SongLiao	902	453	422	604	823	1026	1974
	Yellow	627	472	182	293	525	813	1430
	Yangtze	1706	1039	167	711	1959	2551	3194
	Southwest	496	533	184	212	232	389	1701
	Southeast	2814	881	1781	2160	2550	3262	4570
	Pearl	3846	1822	1564	2604	3320	4698	7512

17

(a) Changes of R-factor (This study - Yin et al., 2019)

-2000 -1000 -500   0   500 1000 2000 4000 6000 8000 10000 $MJ \cdot mm \cdot ha^{-1} \cdot h^{-1} \cdot a^{-1}$

70°0'0"E 80°0'0"E 90°0'0"E 100°0'0"E 110°0'0"E 120°0'0"E 130°0'0"E 140°0'0"E 150°0'0"E

(b) Changes of 1-in-10-year EI_{30} (This study - Yin et al., 2019)

-800 - 500 -250 -100 0 100 250 500 800 1000 1600 $MJ \cdot mm \cdot ha^{-1} \cdot h^{-1}$

295

Figure 9: Differences of the R-factor(a) and the 1-in-10-year EI_{30}(b) comparing with the previous study

Comparing with the maps in Yin et al. (2019), the new maps can be quite different at some local areas (Fig. 9a and 9b). The R-factor in the new map was higher for most of the south-eastern region, and lower for most of the middle and western regions, especially for the south-western area (Fig. 9a). While the 1-in-10-year EI_{30} map shows a similar pattern as that of R-factor,

300   and the overestimation in Yin et al. (2019) seems to be more pronounced for some hilly regions in southeastern China (Fig. 9b).

3.3 Evaluation on the improvement of the erosivity maps

3.3.1 Effect of data temporal resolution

Figure 10 shows that the R-factor estimated from daily data (Eq. 6) is underestimated when the R value is higher than 10,000

305   MJ mm ha^{-1} h^{-1} a^{-1}, and slightly overestimated when the value is lower than 2,000 MJ mm ha^{-1} h^{-1} a^{-1}. The model using hourly data improved the accuracy by about 11.1% (median value of the relative error) compared to that from daily data (Fig. 10).

19

Estimated 1-in-10-year EI_{30} would be underestimated using hourly and daily data, and the underestimation is greater if daily data were used (Fig. 10). Unlike the R-factor, the 1-in-10-year EI_{30} was not noticeably improved with an increase in the temporal resolution from daily to hourly data, probably due to the fact that the 1-in-10-year EI_{30} values estimated using daily
310   data in Yin et al. (2019) had already been multiplied by a conversion factor of 1.17 to correct the 1-in-10-year daily erosivity to approximate the 1-in-10-year event EI_{30} from 1-min data.
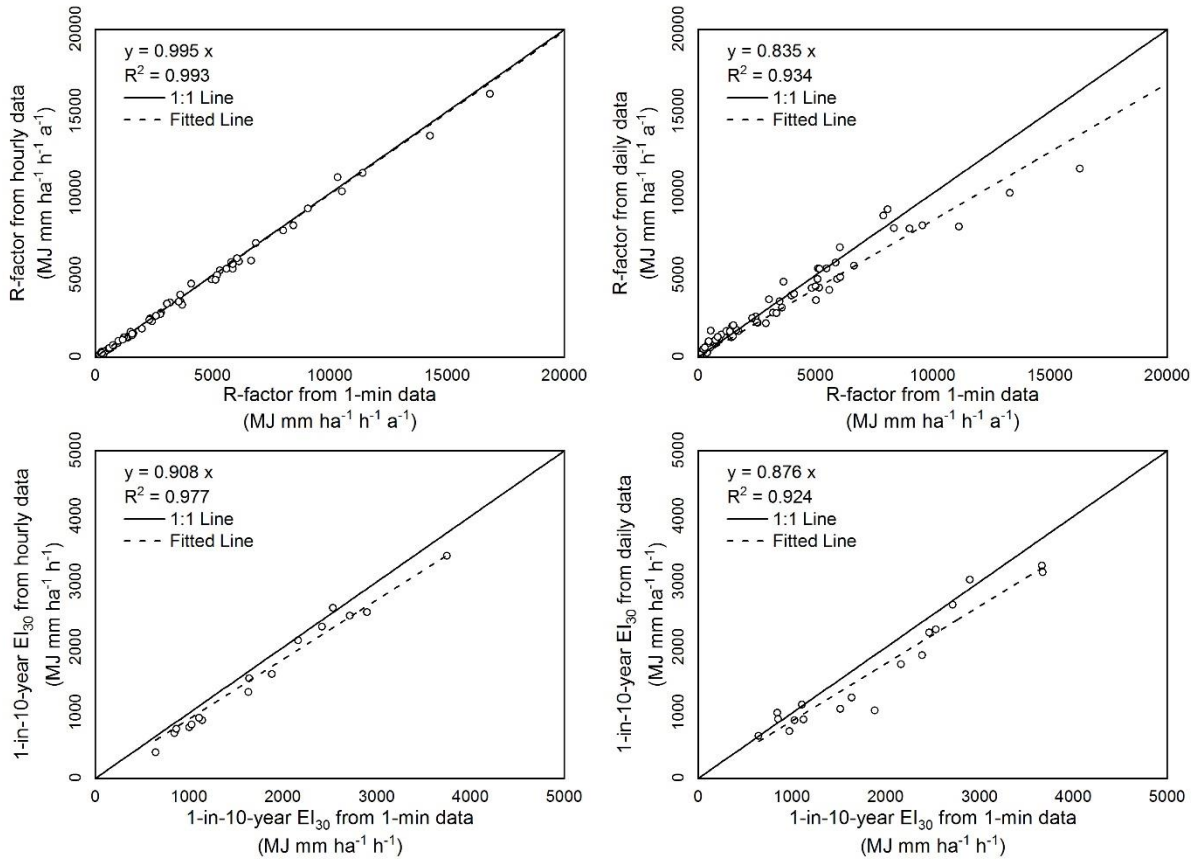
Figure 10: Comparison of the R-factor (upper) and 1-in-10-year EI_{30} (lower) estimated from hourly (left) and daily (right) rainfall data at the stations

315   **3.3.2 Effect of the station density**

Interpolation for the Western (W) region had the lowest NSE value compared to other regions, which may be caused by the low station density (Fig. 1) and the lower spatial correlation of rainfall. The fitted semivariogram for the R-factor in the Western region had a range of 35 km, whereas the ranges for Mid-western (MW), North-eastern (NE) and South-eastern (SE) regions were 288, 261 and 1,235 km, respectively.

20

A comparison of cross-validation between the two maps with different station densities shows that the interpolation with denser stations can improve the accuracy by 2.6% ~ 15.4% for the R-factor based on the sMAPE index, and by 1.4% ~ 31.8% for 1-in-10-year EI_{30} (Table 4) when the station density increased. The NSE can increase by 0.013 to 0.110 for the R-factor. For the 1-in-10-year EI_{30}, the NSE decreased by 0.001 to 0.096 for Western (W), Mid-western (MW) and South-eastern (SE) regions, and increased by 0.038 for the North-eastern (NE) region.

For the R-factor, in the Western (W) region, the station density doubled (increased from 36,600 to 21,200 km^2 per station), and the accuracy improved by 15.4%, whereas the sMAPE of 53.3% was still high with this increase in station density. In the Mid-western (MW) region, the station density tripled (from 13,900 to 4,800 km^2 1 station) and the accuracy was improved by 11.1% based on the sMAPE index from 30.7% to 19.6%. In North-eastern (NE) and South-eastern (SE) regions, the station density tripled and quadrupled, respectively, and the accuracy increased about 2.5%. For 1-in-10-year EI_{30}, the improvement was 31.8% in the Western (W) region and 19.6% in the Mid-western (MW) region. The improvement was mainly in western regions, and the station density in the eastern China before the increase is enough to describe the spatial variation of the R-factor and the 1-in-10-year EI_{30}. It can be inferred that when there were less than about 10,000 km^2 per station, the increasing of the site density has little impact on the improvement of the interpolation (Fig. 11).

Table 4: Comparison of cross-validation results for erosivity maps interpolated based on data from 774 and 2381 stations

Region	No. of the stations	Density of the stations (10^3 km^2 1 station)	R-factor		1-in-10-year EI_{30}	
			sMAPE	NSE	sMAPE	NSE
W	87	36.6	68.7%	0.489	63.7%	0.389
	150	21.2	53.3%	0.599	31.8%	0.293
MW	161	13.9	30.7%	0.938	44.0%	0.887
	471	4.8	19.6%	0.951	24.5%	0.886
NE	214	11.0	12.4%	0.946	17.0%	0.857
	690	3.4	9.7%	0.962	14.9%	0.895
SE	389	6.6	10.9%	0.942	15.5%	0.844
	1362	1.9	8.3%	0.959	14.0%	0.824
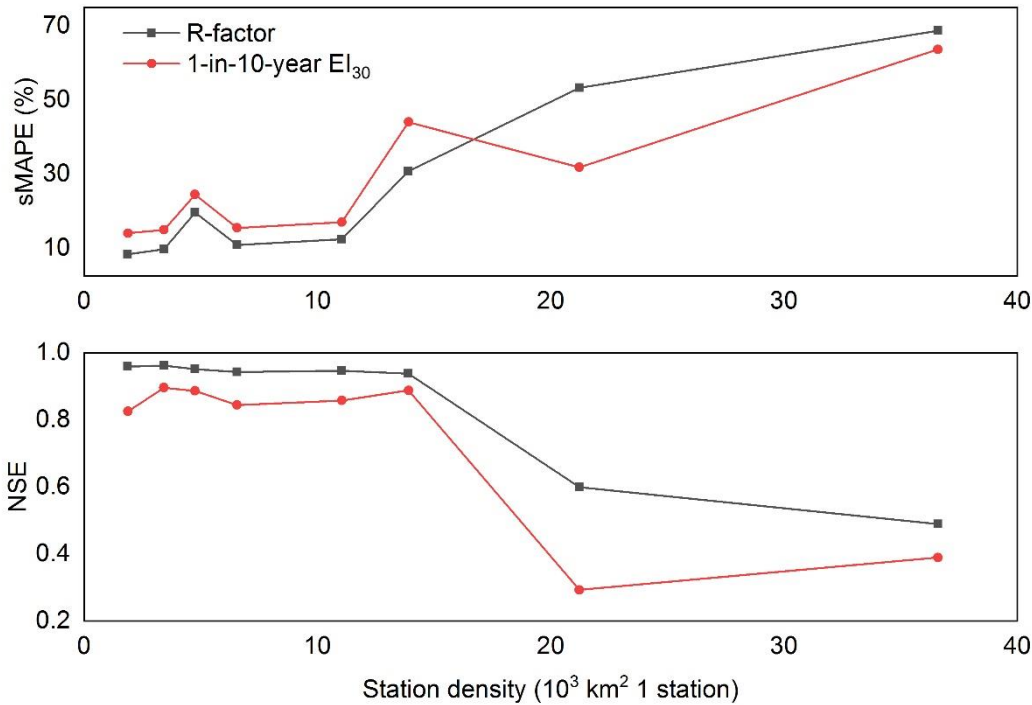
Figure 11: Improvement of the interpolation with the increase of station density. Data were from the 774 and 2381 stations in the 4 different regions

3.3.3 Effect of the interpolation method

For the R-factor, cross-validation of Ordinary Kriging and Universal Kriging with the mean annual rainfall as the co-variable (Table 5) shows that UK improved the interpolation accuracy by 2.3%-9.0% (sMAPE) compared to OK. In the Western (W) region, the NSE increased from 0.285 (OK) to 0.599 (UK). Therefore, it is better to use UK instead of OK when generating the R-factor map, especially in the western China where the station density is low. For the 1-in-10-year EI_{30}, UK improved the accuracy by 0.4%-9.7% (sMAPE). In the Western (W) region, the accuracy improved by 9.7% and the NSE increased from 0.094 (OK) to 0.293 (UK).

Table 5: Cross-validation of the interpolated R-factor and 1-in-10-year event EI_{30} using OK and UK

Region	Interpolation method	R-factor		1-in-10-year EI_{30}	
		sMAPE	NSE	sMAPE	NSE
W	OK	62.3%	0.285	41.5%	0.094
	UK	53.3%	0.599	31.8%	0.293
MW	OK	24.8%	0.861	24.9%	0.838
	UK	19.6%	0.951	24.5%	0.886
NE	OK	12.0%	0.926	16.5%	0.865

22

| Region	Interpolation method	R-factor		1-in-10-year EI_{30}	
		sMAPE	NSE	sMAPE	NSE
	UK	9.7%	0.962	14.9%	0.895
SE	OK	11.2%	0.911	14.8%	0.844
	UK	8.3%	0.959	14.0%	0.824

4 Discussion

This study has produced quality R-factor and 1-in-10-year EI_{30} maps with hourly data from 2,381 stations over mainland China, which are shown to be a noticeable improvement over the maps that are currently available for China (Yin et al., 2019; Table 1). The improvement of the R-factor map over previously published R-factor maps can be attributed to the increase in the temporal resolution from daily to hourly data, whereas that of 1-in-10-year EI_{30} map to the increase of the station density in comparison with those of Yin et al. (2019). There are mainly two reasons for this. First, 1-in-10-year event EI_{30} values estimated from the daily data had already been adjusted to those from the 1-min data by multiplying a conversion factor of 1.17 (Yin et al., 2019), which resulted in no obvious improvement from the daily data to the hourly data. Second, the 1-in-10-year event EI_{30} associated with extreme rainfall event intrinsically has a high spatial variability in comparison to the R-factor as shown in Table 4. The accuracy of spatially interpolated rainfall erosivity was more sensitive to the station density when the station density is low. Hence the improvement of the map of the 1-in-10-year EI_{30} was mainly a result of the increase of the station density, especially for the Western (W) and the Mid-western (MW) regions with a low station density.

Comparison with a world map of rainfall erosivity was also undertaken for mainland China. Panagos et al. (2017) produced a Global Rainfall Erosivity Database with hourly and sub-hourly rainfall data from 3,625 stations from 63 countries. This data base could be used for comparison of rainfall erosivity among different regions in the world. In their study, hourly data from 387 stations in China were used. Figure 12 shows that the R-factor for China extracted from Panagos et al. (2017) is systematically underestimated by about 30% for most areas in China, whereas overestimated in the Tibetan Plateau (cf. Fig. 7a). The reason for the underestimation may be that the R-factor calculated from hourly data applied a conversion factor (CF_{30}) that was developed from the R-factor values computed with 60-min data to those with 30-min data in Panagos et al. (2015b), rather than using an adjustment factor based on breakpoint data (CF_{bp}) or 1-min data (CF_1). Breakpoint data were used for the USLE (Wischmeier and Smith, 1965; 1978), and RUSLE (Renard et al., 1997) and 1-min data for this study. Previous research has shown the difference between CF_{30} and CF_{bp} (CF_1) can result in an underestimation of R-factor by about 20% (Auerswald et al., 2015; Yue et al., 2020). Table 6 shows that the relative error of the map from Panagos et al. (2017) could reduce by about 6.2% after multiplying by a conversion factor of 1.253, which was calibrated by Yue et al. (2020) for converting the R-factor from 30-min data to 1-min data. Because the cross-validation values from the map of Panagos et al. (2017) were not available, values extracted from the maps were used instead to compare with the values from 1-min data at the 62 stations. Erosivity values based on the adjusted maps are still generally underestimated. The reason could be that the equation for estimating the storm energy (E) from rainfall intensity used in Panagos et al. (2017) was from the RUSLE (Renard et al., 1997),

23

and the equation is known to cause underestimation of the storm energy up to 10% in previous studies (Mcgregor et al., 1995;

375 Yin et al., 2017). Because of this, the equation for estimating the storm energy (E) in RUSLE (Renard et al., 1997) was then modified in RUSLE2 (USDA-ARS, 2013), which was adopted in this study.

The R-factor in the Tibetan Plateau varies from 0 to 12,326 MJ mm ha^{-1} h^{-1} a^{-1} in Panagos et al. (2017), and from 5 to 4,442 MJ mm ha^{-1} h^{-1} a^{-1} in this study. The former was derived from a Gaussian Process Regression (GPR) model and a number of monthly climate variables from the WorldClim database, such as the mean monthly precipitation, mean minimum, average

380 and maximum monthly temperature. The GPR model was calibrated using the site-specific R-factor values and these climate variables, which may not applicable for sites at high altitude, as none of the observation sites was located in the Tibetan Plateau region. The GPR model might be the main reason for the overestimation of the R-factor in the Tibetan Plateau where the R-factor was expected to be underestimated just like any other regions.
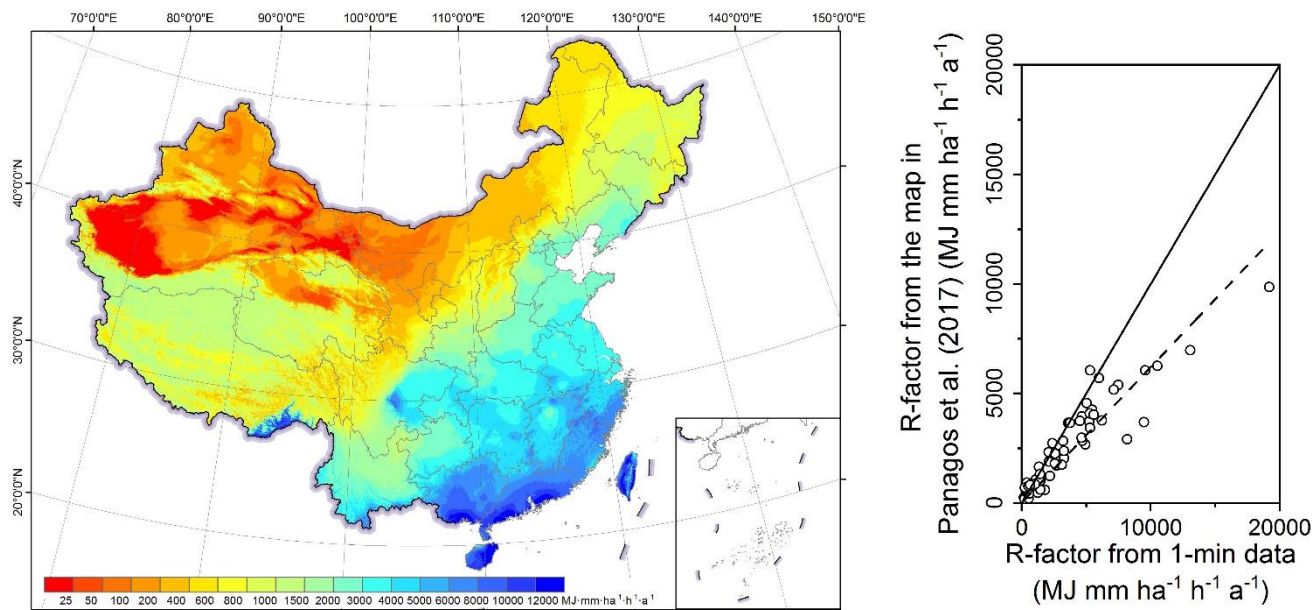
385 **Figure 12: R-factor map for China extracted from Panagos et al. (2017) and the evaluation of the map based on 62 stations with 1-min data.**

Table 6: Comparison of the statistical characteristics of the relative errors of the R-factor extracted from the map generated in this study and extracted from Panagos et al. (2017) (original and adjusted). The adjusted map of Panagos et al. (2017) was the original

390 **map multiplying by a conversion factors of 1.253, which was calibrated by Yue et al. (2020) for converting the R-factor from 30-min data to 1-min data.**

	This study	Panagos et al. (2017)	Panagos et al. (2017) adjusted
25th percentile	7.1%	14.8%	10.4%
Median	16.1%	28.3%	22.1%
75th percentile	28.0%	40.5%	43.2%
Mean	20.1%	33.8%	33.1%

24

Although this study provides improved erosivity maps in comparison with previous studies, errors remain inevitably. The uncertainty of the estimated R-factor and 1-in-10-year erosivity values from this study mainly comes from the following sources: First, KE-I model for estimating Kinetic Energy (KE) from the precipitation Intensity (I). KE-I model used in this study is from RUSLE2 (USDA-ARS, 2013) and raindrop disdrometer observation data need to be collected to calibrate the KE-I relationship. Second, estimation of the erosivity factors was based on hourly data, and conversion factors were developed based on 1-min rainfall data from 62 stations (Fig. 2). Hourly data brings information loss in the estimation of instant precipitation intensity comparing with breakpoint data. Third, the adjustment of the R-factor for the stations with a small number of effective years (Eq. 7). This was based on a power function relationship (Eq. 8) between the mean annual precipitation and rainfall erosivity using 1-min and daily rainfall data of 35 stations. The magnitude of uncertainty mainly depends on the variation of annual rainfall erosivity. Forth, station distribution and density. In western China, the stations were sparsely and unevenly distributed, which affect the interpolation accuracy. Finally, spatial interpolation technique (Universal Kriging in this study) and the interpolation procedures, i.e. the division of regions before the interpolation and the mergence of regions after the interpolation. These five sources of uncertainty need to be addressed for any further improvement in erosivity estimation in China.

5 Conclusions

This study has generated new R-factor and 1-in-10-year EI_{30} maps using hourly and daily rainfall data for the period from 1951 to 2018 from 2,381 stations over mainland China. The improvement in the accuracy of these erosivity maps over what are currently available was evaluated in terms of the median absolute relative error, and was explained in terms of temporal resolution of data used, station density, and interpolation methods. The following conclusions can be drawn from this study:

(1) Comparing with the existing maps for the 62 reference sites, the median absolute relative error in the R-factor map generated in this study was reduced from 18.1% to 17.8% for the mid-western and eastern regions, from 161.6% to 16.2% for the western region, and for the 1-in-10-year EI_{30}, from 20.6% to 13.5% in the mid-western and eastern regions.

(2) The R-factor value varied from 0 to 25,300 MJ mm ha^{-1} h^{-1} a^{-1}, and the 1-in-10-year EI_{30} value was from 0 to 11,246 MJ mm ha^{-1} h^{-1}. In comparison with the existing maps, new maps of the R-factor and 1-in-10-year event EI_{30} show a clear decreasing trend from south-eastern to north-eastern China.

(3) Improvement in the R-factor map can be mainly attributed to an increase in the temporal resolution from daily to hourly, whereas that in the 1-in-10-year EI_{30} map to an increase of the station density. The increased station density has led to an improved R-factor and 1-in-10-year EI_{30} maps for the western regions primarily. The benefit from an increased station density is limited once the station density reached about 1 station per 10,000 km^2. As for the interpolation method, Universal Kriging with the mean annual rainfall as the co-variable performed better than Ordinary Kriging for all regions, especially for the western regions with sparse weather stations.

Competing interests

The authors declare that they have no conflict of interest.

References

Alewell, C., Borelli, P., Meusburger, K., and Panagos, P.: Using the USLE: Chances, challenges and limitations of soil erosion
435   modelling, International soil and water conservation research, 203-225, doi:10.1016/j.iswcr.2019.05.004, 2019.

Angulomart ńez, M. and Beguer á, S.: Estimating rainfall erosivity from daily precipitation records: A comparison among methods using data from the Ebro Basin (NE Spain), Journal of Hydrology, 379, 111-121, doi:10.1016/j.jhydrol.2009.09.051, 2009.

Arnoldus, H.: Methodology used to determine the maximum potential average annual soil loss due to sheet and rill erosion in
440   Morocco, FAO Soils Bulletins (FAO), 34, 39-51, 1977.

Auerswald, K., Fiener, P., Gomez, J. A., Govers, G., Quinton, J. N., and Strauss, P.: Comment on "Rainfall erosivity in Europe" by Panagos et al. (Sci. Total Environ., 511, 801-814, 2015), Science of the Total Environment, 532, 849-852, doi:10.1016/j.scitotenv.2015.05.019, 2015.

Bagarello, V. and D'Asaro, F.: Estimating single storm erosion index, Transactions of the ASAE, 37, 785-791,
445   doi:10.13031/2013.28141, 1994.

Bonilla, C. A. and Vidal, K. L.: Rainfall erosivity in central Chile, Journal of Hydrology, 410, 126-133, doi:10.1016/j.jhydrol.2011.09.022, 2011.

Borrelli, P., Diodato, N., and Panagos, P.: Rainfall erosivity in Italy: a national scale spatio-temporal assessment, International Journal of Digital Earth, 9, 835-850, doi:10.1080/17538947.2016.1148203, 2016.

450   Capolongo, D., Diodato, N., Mannaerts, C., Piccarreta, M., and Strobl, R.: Analyzing temporal changes in climate erosivity using a simplified rainfall erosivity model in Basilicata (southern Italy), Journal of Hydrology, 356, 119-130, doi:10.1016/j.jhydrol.2008.04.002, 2008.

Coles, S. G.: An introduction to statistical modeling of extreme values. - springer, Series in Statistics, doi:10.1007/978-1-4471-3675-0, 2001.

455   FAO: Soil erosion: the greatest challenge to sustainable soil management, Rome, 2019a.

FAO: Outcome document of the Global Symposium on Soil Erosion, Rome, 2019b.

Ferrari, R., Pasqui, M., Bottai, L., Esposito, S., and Di Giuseppe, E.: Assessment of soil erosion estimate based on a high temporal resolution rainfall dataset, Proc. 7th European Conference on Applications of Meteorology (ECAM), Utrecht, Netherlands, 12-16,

460   Ferro, V., Giordano, G., and Iovino, M.: Isoerosivity and erosion risk map for Sicily, Hydrological Sciences Journal, 36, 549-564, doi:10.1080/02626669109492543, 1991.

Haith, D. A. and Merrill, D. E.: Evaluation of a daily rainfall erosivity model, Transactions of the ASAE, 30, 0090-0093, doi:10.13031/2013.30407, 1987.

Hosking, J. R. M.: L-Moments: Analysis and Estimation of Distributions Using Linear Combinations of Order Statistics,
465   Journal of the Royal Statistical Society, 52, 105-124, doi:10.2307/2345653, 1990.

Klik, A., Haas, K., Dvorackova, A., and Fuller, I. C.: Spatial and temporal distribution of rainfall erosivity in New Zealand, Soil Research, 53, 887-901, doi:10.1071/SR14363, 2015.

Lee, J. H. and Heo, J. H.: Evaluation of Estimation Methods for Rainfall Erosivity Based on Annual Precipitation in Korea, Journal of Hydrology, 409, 30-48, doi:10.1016/j.jhydrol.2011.07.031, 2011.

470   Li, T., Zheng, X., Dai, Y., Yang, C., Chen, Z., Zhang, S., Wu, G., Wang, Z., Huang, C., and Shen, Y.: Mapping near-surface air temperature, pressure, relative humidity and wind speed over Mainland China with high spatiotemporal resolution, Advances in Atmospheric Sciences, 31, 1127-1135, doi:10.1007/s00376-014-3190-8, 2014.

Liu, B., Tao, H., and Song, C.: Temporal and spatial variations of rainfall erosivity in China during 1960 to 2009, Geographical Research, 32, 245-256, doi:10.11821/yj2013020005, 2013.

475   Liu, Y., Zhao, W., Liu, Y., and Pereira, P.: Global rainfall erosivity changes between 1980 and 2017 based on an erosivity model using daily precipitation data, CATENA, 194, 104768, doi:10.1016/j.catena.2020.104768, 2020.

Lu, H. and Yu, B.: Spatial and seasonal distribution of rainfall erosivity in Australia, Soil Research, 40, 887-901, doi:10.1071/SR01117, 2002.

McGregor, K., Bingner, R., Bowie, A., and Foster, G.: Erosivity index values for northern Mississippi, Transactions of the
480   ASAE, 38, 1039-1047, doi:10.13031/2013.27921, 1995.

Naipal, V., Reick, C. H., Pongratz, J., and Van Oost, K.: Improving the global applicability of the RUSLE model-adjustment of the topographical and rainfall erosivity factors, Geoscientific Model Development Discussions, 8, 2991-3035, doi:10.5194/gmdd-8-2991-2015, 2015.

Oliveira, P. T. S., Rodrigues, D. B. B., Sobrinho, T. A., Carvalho, D. F. D., and Panachuki, E.: Spatial variability of the rainfall erosive potential in the State of Mato Grosso do Sul, Brazil, Engenharia Agrícola, 32, 69-79, doi:10.1590/S0100-69162012000100008, 2012.

Panagos, P., Ballabio, C., Borrelli, P., and Meusburger, K.: Spatio-temporal analysis of rainfall erosivity and erosivity density in Greece, Catena, 137, 161-172, doi:10.1016/j.catena.2015.09.015, 2015a.

Panagos, P., Ballabio, C., Borrelli, P., Meusburger, K., Klik, A., Rousseva, S., Tadić, M. P., Michaelides, S., and Hrabalíková, M.: Rainfall erosivity in Europe, Science of the Total Environment, 511, 801-814, doi:10.1016/j.scitotenv.2015.01.008, 2015b.

Panagos, P., Borrelli, P., Meusburger, K., Yu, B., Klik, A., Lim, K. J., Yang, J. E., Ni, J., Miao, C., and Chattopadhyay, N.: Global rainfall erosivity assessment based on high-temporal resolution rainfall records, Scientific Reports, 7, 4175, doi:10.1038/s41598-017-04282-8, 2017.

Qin, W., Guo, Q., Zuo, C., Shan, Z., Ma, L., and Sun, G.: Spatial distribution and temporal trends of rainfall erosivity in mainland China for 1951–2010, Catena, 147, 177-186, doi:10.1016/j.catena.2016.07.006, 2016.

Renard, K. G. and Freimund, J. R.: Using monthly precipitation data to estimate the R-factor in the revised USLE, Journal of Hydrology, 157, 287-306, doi:10.1016/0022-1694(94)90110-4, 1994.

Renard, K. G., Foster, G. R., Weesies, G. A., Mccool, D. K., and Yoder, D. C.: Predicting soil erosion by water: a guide to conservation planning with the Revised Universal Soil Loss Equation (RUSLE), Agricultural Handbook, USDA-Agricultural Research Service, Washington, D.C.1997.

Richardson, C., Foster, G., and Wright, D.: Estimation of erosion index from daily rainfall amount, Transactions of the ASAE, 26, 0153-0156, doi:10.13031/2013.33893, 1983.

Riquetti, N. B., Mello, C. R., Beskow, S., and Viola, M. R.: Rainfall erosivity in South America: Current patterns and future perspectives, Science of The Total Environment, 724, 138315, doi:10.1016/j.scitotenv.2020.138315, 2020.

Sadeghi, S. H., Zabihi, M., Vafakhah, M., and Hazbavi, Z.: Spatiotemporal mapping of rainfall erosivity index for different return periods in Iran, Natural Hazards, 87, 35-56, doi:10.1007/s11069-017-2752-3, 2017.

Selker, J. S., Haith, D. A., and Reynolds, J. E.: Calibration and testing of a daily rainfall erosivity model, Transactions of the ASAE, 33, 1612, doi:10.13031/2013.31516, 1990.

Sheridan, J., Davis, F., Hester, M., and Knisel, W.: Seasonal distribution of rainfall erosivity in peninsular Florida, Transactions of the ASAE, 32, 1555-1560, doi:10.13031/2013.31189, 1989.

Silva, R. M., Santos, C., Silva, J., Silva, A. M., and Neto, R.: Spatial distribution and estimation of rainfall trends and erosivity in the Epitácio Pessoa reservoir catchment, Paraíba, Brazil, Natural Hazards: Journal of the International Society for the Prevention and Mitigation of Natural Hazards, 102, doi:10.1007/s11069-020-03926-9, 2020.

USDA-ARS: Science documentation: Revised Universal Soil Loss Equation Version 2 (RUSLE2), USDA-Agricultural Research Service, Washington, D.C., 2013.

Wang, W., Jiao, J., Hao, X., Zhang, X., and Lu, X.: Distribution of rainfall erosivity R value in China, Journal of Soil Erosion and Soil Conservation, 29-39, 1996.

Wischmeier, W. H.: A Rainfall Erosion Index for a Universal Soil-Loss Equation 1, Soil Science Society of America Journal, 23, 246-249, doi:10.2136/sssaj1959.03615995002300030027x, 1959.

520 Wischmeier, W. H. and Smith, D. D.: Rainfall energy and its relationship to soil loss, Trans. Am. Geophys. Union, 39, 285-291, doi:10.1029/tr039i002p00285, 1958.

Wischmeier, W. H. and Smith, D. D.: Predicting rainfall-erosion losses from cropland east of the Rocky Mountains: Guide for selection of practices for soil and water conservation, Agricultural Handbook, USDA-Agricultural Research Service, Washington, D.C.1965.

525 Wischmeier, W. H. and Smith, D. D.: Predicting rainfall erosion losses - a guide to conservation planning, Agricultural Handbook, USDA-Agricultural Research Service, Washington, D.C.1978.

Xie, Y., Liu, B. Y., and Zhang, W. B.: Study on standard of erosive rainfall, Journal of Soil & Water Conservation, 14, 6-11, doi:10.13870/j.cnki.stbcxb.2000.04.002, 2000.

Xie, Y., Yin, S. Q., Liu, B. Y., Nearing, M. A., and Zhao, Y.: Models for estimating daily rainfall erosivity in China, Journal

530 of Hydrology, 535, 547-558, doi:10.1016/j.jhydrol.2016.02.020, 2016.

Yin, S., Nearing, M. A., Borrelli, P., and Xue, X.: Rainfall Erosivity: An Overview of Methodologies and Applications, Vadose Zone Journal, 16, doi:10.2136/vzj2017.06.0131, 2017.

Yin, S., Xie, Y., Liu, B., and Nearing, M. A.: Rainfall erosivity estimation based on rainfall data collected over a range of temporal resolutions, Hydrology and Earth System Sciences, 19, 4965-4996, doi:10.5194/hess-19-4113-2015, 2015.

535 Yin, S., Xue, X., Yue, T., Xie, Y., and Gao, G.: Spatiotemporal distribution and return period of rainfall erosivity in China, Transactions of the Chinese Society of Agricultural Engineering, 35, 105-113, doi:10.11975/j.issn.1002-6819.2019.09.013, 2019.

Yu, B. and Rosewell, C. J.: Technical notes: a robust estimator of the R-factor for the universal soil loss equation, Transactions of the ASAE, 39, 559-561, doi:10.13031/2013.27535, 1996a.

540 Yu, B. and Rosewell, C. J.: Rainfall erosivity estimation using daily rainfall amounts for South Australia, Soil Research, 34, 721-733, doi:10.1071/SR9960721, 1996b.

Yu, B. and Rosewell, C. J.: An assessment of a daily rainfall erosivity model for New South Wales, Australian Journal of Soil Research, 34, 139-152, doi:10.1071/SR9960139, 1996c.

Yue, T., Xie, Y., Yin, S., Yu, B., Miao, C., and Wang, W.: Effect of time resolution of rainfall measurements on the erosivity

545 factor in the USLE in China, International Soil and Water Conservation Research, 8, 373-382, doi:10.1016/j.iswcr.2020.06.001, 2020.

Zhang, W., Xie, Y., and Liu, B.: Rainfall Erosivity Estimation Using Daily Rainfall Amounts, Scientia Geographica Sinica, 22, 53-56, doi:10.13249/j.cnki.sgs.2002.06.012, 2002.

Zhang, W., Xie, Y., and Liu, B.: Spatial distribution of rainfall erosivity in China, Journal of Mountain Science, 21, 33-40,

550 doi:10.16089/j.cnki.1008-2786.2003.01.005, 2003.

Zhu, Z. and Yu, B.: Validation of Rainfall Erosivity Estimators for Mainland China, Transactions of the ASABE, 58, 61-71, doi:10.13031/trans.58.10451, 2015.